Applied Catalysis B: Environmental 220 (2018) 581–588

Contents lists available at ScienceDirect

Applied Catalysis B: Environmental

journal homepage: www.elsevier.com/locate/apcatb

Structurally tuning microwave absorption of core/shell structured CNT/polyaniline catalysts for energy efficient saccharide-HMF conversion

Tuo Ji[a], Rui Tu[b], Liwen Mu[a], Xiaohua Lu[b], Jiahua Zhu[a,*]

[a] Intelligent Composites Laboratory, Department of Chemical and Biomolecular Engineering, The University of Akron, Akron, OH 44325, USA
[b] State Key Laboratory of Material-Oriented Chemical Engineering, College of Chemistry and Chemical Engineering Department, Nanjing Tech University, Nanjing, 210009, PR China

ARTICLE INFO

Keywords:
Biomass
5-Hydroxymethylfurural
Heterogeneous catalyst
Microwave absorption
Sustainability

ABSTRACT

Microwave absorption and catalytic activity have been synergistically integrated into a core/shell structured CNT/polyaniline (PANI) hybrid catalyst that enables localized heating on the catalyst surface and uplifts energy efficiency in the dehydration reaction of saccharides to 5-hydroxymethylfurfural (HMF). Results reveal that the integration of CNT and polyaniline significantly improves the overall saccharide conversion and HMF yield. The PANI shell thickness and morphology are controlled by both reactant feeding ratio and polymerization reaction rate. A thinner and rougher PANI shell is favourable to enhance the overall microwave absorption, improve heat transfer efficiency to catalyst surface and thus reaction efficiency. The highest energy efficiency of 7.6 mmol kJ^{-1} L^{-1} is reached in 10 min with CNT/PANI catalyst (30 wt% CNTs) and 19 W input power. Moreover, the packing of polyaniline shell on CNT core facilitates its separation from reaction mixture and effectively prevents catalyst loss. These catalysts show excellent recyclability that the catalyst activity can be completely recovered by a simple re-doping process in 1.0 M sulfuric acid. This work opens up a new window in microwave responsive catalyst design that enhances energy efficiency in saccharide-HMF conversion reactions and promotes the economic feasibility of such reactions in practice.

1. Introduction

Exploration of sustainable energy is becoming one of the most pursuing research areas in this century facing the challenge of fossil fuel depletion [1]. The sustainable nature of biomass resources attracts great interests in catalysis, energy storage, environmental remediation, and especially in the synthesis of valuable platform chemicals [2–7]. Among them, synthesis of 5-hydroxymethylfurfural (HMF) from carbohydrate (*e.g.* cellulose, saccharide) is the most studied reaction and it is considered as an important step in biomass utilization that leads to a variety of valuable chemicals [8,9]. For example, HMF can be rehydrated to levulinic acid or oxidized to furandicarboxylic acid [10,11]. Until now, different catalysts, such as Nb_2O_5 [12], SO_4^{2-}/ZrO_2 [13], and $VOPO_4$-SiO_2 [14] have been developed to maximize the HMF yield by using saccharide as reactant [15]. However, a few major disadvantages of existing reaction systems, such as low HMF yield in aqueous medium, long reaction time, high energy consumption and potential environmental issues by using organic solvent, restrict their further development into practical stage. For instance, using aprotic organic solvent in the reaction can boost HMF yield and suppress side-reactions, but it comes with a separation process that often consumes a great amount of energy not even mention the potential environmental pollutions. For the selection of catalyst, heterogeneous catalysts could be more advantageous than homogeneous catalysts in terms of easy separation and low risk of corrosion to equipment. However, previous studies revealed that heterogeneous catalysts are easy to lose their activity and the subsequent separation and reactivation processes are often complicated [16].

Conventional dehydration reaction of saccharides often requires long reaction time of several hours or even longer at high temperature. To expedite reaction rate and improve energy efficiency, microwave heating has been used in such reactions [17,18]. In theory, microwave irradiation is able to generate hot-spots in the reaction medium and provide localized heating to accelerate the reaction [19,20]. For example, Carrasquillo-Flores et al. achieved 91% yield of glucose and 96% yield of xylose in the depolymerization reaction of cellulose by using microwave, which is about 6 times the yield compared to conventional heating method at the same reaction condition [21]. Qi et al. found that not only the fructose conversion was improved by using microwave, the 5-HMF yield is also increased in the presence of a cation exchange resin

* Corresponding author.
E-mail address: jzhu1@uakron.edu (J. Zhu).

http://dx.doi.org/10.1016/j.apcatb.2017.08.066
Received 17 February 2017; Received in revised form 29 May 2017; Accepted 18 August 2017
Available online 24 August 2017

catalyst [22]. Realizing the fact that most of existing heterogeneous catalysts (*e.g.* TiO_2, Niobic acid and Amberlyst-15) are microwave-transparent [23]. The catalyst itself does not absorb microwave and it does not contribute to the heating of the reaction system. The heat generated from the reaction is mainly contributed by polar solvent such as water. However, all heterogeneous reactions occur at the surface of the catalyst. Localized heat generation from catalyst could be more advantageous in terms of the heat utilization during reaction. Until now, the coupling of microwave irradiation and catalyst design has rarely been investigated.

In a heterogeneous catalytic reaction, microwave energy could be absorbed by both solid catalyst and liquid media by careful material design in the reaction system. The heat generation efficiency depends on many factors including but not limit to the dielectric/electric properties (*e.g.* complex permittivity and complex permeability) and interface structure of the solid catalyst [24,25]. To expedite the reaction at catalyst surface, it is preferred to allocate more microwave energy to the surface of solid catalyst where reaction occurs. Carbon materials, such as carbon nanotubes (CNTs) [26,27], carbon black [28], graphene [29], and carbon fibers (CFs) [30], are ideal microwave absorbers due to their excellent dielectric polarization properties. However, the inert surface property of carbon materials disqualifies them as suitable catalyst. Even though acidification of carbon materials could be an alternative approach to introduce catalytic function, this process damages the conjugated pi-pi structure of carbon and therefore disables its microwave-absorption property [31,32]. Therefore, integrating carbon material and functional catalyst could be an effective approach to obtain efficient microwave responsive catalyst with sufficient acid sites. Polyaniline (PANI), a well-studied conducting polymer, acquires two major advantages as microwave catalyst. One is the good electrical conductivity and dielectric loss, which ensure excellent microwave absorption property [33]. The other is its abundant acid sites and convenient doping of different acids [34]. For example, Drelinkiewicz et al. used organo-sulfonic acid doped polyaniline as catalyst in transesterification and esterification reactions, where the yield of methyl esters reached up to 90 mol% in 6 h [35].

In this work, microwave responsive core/shell structured hybrid catalysts were successfully synthesized with carbon nanotubes (CNTs) as microwave absorber core and polyaniline (PANI) as catalytically active shell. These catalysts were studied in the microwave-assisted dehydration reaction from saccharides to HMF. The polyaniline shell thickness and structure were controlled to study their effects on microwave absorption as well as catalytic properties. By controlling the input power of microwave irradiation, the microwave absorption capability and catalytic reactivity of such core/shell structured catalysts were evaluated. Finally, the separation and activation of these catalysts were studied in multiple reaction cycles.

2. Experimental

2.1. Materials

CNTs (Pyrograf III PR-24-XT-LHT, d ≈ 50–100 nm, length: 50–200 μm) was obtained from Pyrograf Products Inc. Aniline ($C_6H_7N \geq 99.5\%$), Ammonium persulfate (APS ≥ 98%), D-(−)-fructose ($C_6H_{12}O_6 \geq 99\%$), D-(+)-glucose ($C_6H_{12}O_6 \geq 99.5\%$) and sucrose ($C_{12}H_{22}O_{11}$) were purchased from Sigma-Aldrich. 2,4-pentanedione (≥99%) was purchased from Acros Organics. Sulfuric acid (98%) was purchased from Fisher Scientific. Ethanol (200 proof) was purchased from Decon Laboratories, Inc. All reagents were used as received without further purification. Deionized water was purified using a Milli-Q Direct 8 Ultrapure Water system (Millipore, Billerica, MA) with a minimum resistivity of 18.2 MΩ cm and used for all experiments.

2.2. Surface modification of CNTs

CNTs were modified to introduce surface functional groups, *e.g.* −OH and −COOH. Briefly, 1.0 g CNTs were added into 50 mL 1.7 M APS and 2.0 M H_2SO_4 mixture solution and ultra-sonicated in a water bath for 3 h. Upon completion, the mixture was kept in an oven at 50 °C for 17 h. Finally, the functionalized CNTs were rinsed by 100 mL DI water for three times and dried in oven at 60 °C overnight.

2.3. Synthesis of polyaniline and CNT/PANI catalysts

Core/shell structured CNT/PANI catalysts were synthesized by using a surface-initiated polymerization method [36]. Specifically, certain amount of modified CNTs (0.10, 0.25, 0.43 and 0.66 g representing 10, 20, 30 and 40 wt% of CNTs in the CNT/PANI composites) were initially mixed with aniline/H_2SO_4 solution (11 mmol aniline in 30 mL 1.0 M H_2SO_4) and then sonicated for 1 h. Then, a mixture of 10 mL 1.3 mmol APS solution and 10 mL 1.0 M H_2SO_4 was added dropwise into the above suspension. Polymerization reaction was carried out at 4 °C for 20 h. The resulting solids were rinsed with DI water until the filtrate became neutral and then dried at 60 °C. The products were named CP10, CP20 CP30 and CP40 where the numbers represented the weight percentage of CNTs in the CNT/PANI composites. Pure PANI was synthesized following the same procedures without adding CNTs. To control the polymerization reaction, the amount of APS was tuned at 0.4, 1.3, 2.2 and 3.1 mmol while synthesizing CP30 and the products were named as CP30-0, CP30-1, CP30-2 and CP30-3, respectively.

2.4. Characterizations

Catalyst morphology was characterized by scanning electron microscopy (SEM, JEOL-7401, 5 kV) with a sputter-coated silver layer on sample surface. The shell thickness and crystal lattice structure were further characterized by transmission electron microscopy (FEI Scanning TEM) and high resolution TEM (HRTEM, FEI Tecnai G2 F20 ST TEM/STEM & EDAX energy dispersive x-ray spectrometer) at 200 kV. Samples for TEM characterization were prepared by drying a drop of sample powder ethanol suspension on carbon-coated copper TEM grids. The powder X-ray diffraction analysis was carried out with a Bruker AXS D8 Discover diffractometer with GADDS (General Area Detector Diffraction System) operating with a Cu-K α radiation source filtered with a graphite monochromator (λ = 1.541 Å). Brunauer–Emmett–Teller (BET) surface area analysis was measured using a TriStar II 3020 surface analyser (Micromeritics Instrument Corp., USA) by N_2 adsorption–desorption isotherms at 77 K. These samples were pre-treated by N_2 flow at 80 °C for 12 h. The pore size distribution was calculated by the Barrett-Joyner-Halenda (BJH) method from the adsorption branch. Elemental analysis of CNT/PANI for C, S and N was performed using a FLASH EA-1112A elemental analyser.

2.5. Catalytic reaction under microwave irradiation

The dehydration reactions were carried out in a microwave tube (10 mL, ID = 12 mm) under microwave irradiation. Typically, 0.55 mmol saccharide and 50 mg CNT/PANI catalyst were added into 4.0 mL water and then sonicated for 5 min. A small stirrer bar was used for mixing during microwave reaction. The loaded tube was then placed into the microwave reactor (Discover SP, CEM) and been exposed to 15 W microwave power for 30 min. After that, the system temperature cooled down to room temperature. The system temperature was measured by infrared technique. The resulting solution was filtered using a syringe filter (VWR, 0.22 mm PTFE). The filtrate was then analyzed by both UV–vis spectrophotometry and HPLC equipped with RI detector and HPX-87 column with 0.17 mL/min of distilled water at 55 °C. The

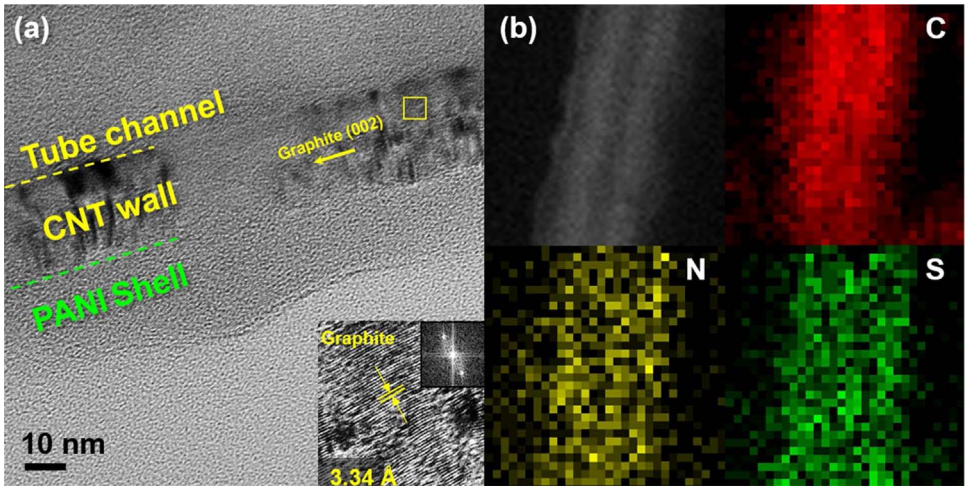

Fig. 1. (a) HRTEM image of CP30, inset figure is magnified CNTs wall and PANI shell, (b) Zero-loss image of CP30 and the corresponding energy filtered TEM of C, N and S elements.

fructose conversion and HMF yield were calculated by Eqs. (1) and (2):

$$Fructose\ \ conversion(\%) = \frac{Fructose\ \ consumed(mol)}{Initial\ \ fructose(mol)} \times 100 \quad (1)$$

$$HMF\ \ yield(\%) = \frac{HMF\ \ produced(mol)}{Initial\ \ fructose(mol)} \times 100 \quad (2)$$

3. Results and discussion

High-resolution TEM (HRTEM) image confirms the core/shell structure of CNT/PANI composite, Fig. 1. The CNTs wall shows a high crystalline structure with an interplanar spacing of 3.34 Å. Such clear lattice fringe and FFT image indicate the well-crystallized (002) plane of graphite (JCPDS #01-0646) [37]. XRD results show intense graphitic peaks ever after growing PANI that clearly indicates the well-reserved crystalline structure of CNTs, Fig. S1. As noticed, the PANI layer is tightly packed on CNTs wall with a thickness of about 20 nm. Such compact structure is especially useful in heat transfer and microwave transmission across the interface [38]. Energy-filtered TEM was conducted on CP30 to characterize the distribution of C, N and S elements. The C element is concentrated in the central area of the composite that represents the CNTs. N and S elements cover a wider area all through material indicating the uniform coating of PANI layer on top of CNTs core. The similar pattern of N and S elements also reveals a good coverage of doping acids on PANI shell.

The PANI shell structure and thickness are critical in determining the overall microwave absorption and surface active sites for reaction. In this work, PANI layer thickness was adjusted by simply controlling the ratio of CNTs and PANI during catalyst synthesis. Fig. 2(a–d) shows the TEM images of CNT/PANI composites with continuously increasing CNTs loading. Pure CNTs has a smooth surface and the diameter is in the range of 50–100 nm, Fig. S2. After polymerization, a uniform layer of flake-like PANI was formed surrounding the CNTs' external surface. The layer thickness and morphology depend on the ratio of PANI and CNTs. With increasing CNTs ratio from 10 to 30 wt%, the average shell thickness decreases from 122 ± 11 to 74 ± 6 and 34 ± 5 nm, respectively. Further increasing CNT ratio to 40 wt% leads to an incomplete surface coverage of PANI, Fig. S3. Smaller CNT ratio not only produces a thicker PANI layer, but also increases its surface roughness. The flake pattern becomes sharp-ended that creates extra free space in the shell. Such structure is beneficial to reflect microwave energy into the core-shell structure, improve the overall microwave absorption and thus enhance energy efficiency of the reaction [39].

N_2 adsorption-desorption isotherms are conducted to characterize the pore structure and surface area of the CNT/PANI composites, Fig. S4. Table 1 summarizes the structural feature and elemental composition of CNTs, PANI and CNT/PANI composites. Generally, the introduction of CNTs slightly increases the surface area of composites from 23.5 to 29.0 $m^2\ g^{-1}$ while the pore volume and pore size are similar for all the materials. With increasing CNTs percentage, the ratio of nitrogen element decreases gradually from 4.3 to 1.8 wt% due to the increased portion of carbon in the composite. By analyzing the sulfur composition, it seems that CP10, CP20 and CP30 have similar amount of sulfur at about 3 wt%, which could be attributed to the out-surface doping of PANI rather than bulk doping. While in CP40, the incomplete surface coverage of PANI leads to lower sulfur content to 1.7 wt%.

The potential benefits of the integration of CNTs core and PANI shell in the hybrid microwave responsive catalysts are firstly screened by equilibrium system temperature, fructose conversion and HMF yield. As for the temperature profile in Fig. 3(a), all the materials including pure water start with a sharp increase of temperature in the first a couple of minutes and then the curves become flat at different equilibrium temperatures. Pure water, as a control, shows the lowest equilibrium temperature of 118 °C simply because water is the only microwave absorber in the system. Adding CNTs, PANI and CNT/PANI into the system shift the equilibrium temperature to higher values (PANI: 145 °C; CNTs: 171 °C; CNT/PANI: 158 °C). The highest equilibrium temperature is reached by CNTs due to its excellent microwave absorption property taking advantage of its large aspect ratio (> 500) and conjugated graphitic structure [40,41]. However, high system temperature does not necessarily guarantee a better reaction efficiency. For example, HMF yield and fructose conversion are 31 mol% and 52 mol %, respectively, by using CNTs as catalyst. Even higher HMF yield of 46 mol% and fructose conversion of 61 mol% was reached by pure PANI catalyst. By integrating CNTs and PANI (CP30), HMF yield of 69 mol% and fructose conversion of 81 mol% can be achieved. In this work, the integrated core/shell structure enables both improved equilibrium temperature and maximized active sites for reaction. Even though previous research reported that the integration of CNTs and PANI could increase both dielectric and magnetic loss compared to pure CNTs and therefore generate more heat under microwave radiation [42,43], the relatively lower equilibrium temperature of CP30 than that of CNTs could be attributed to the low thermal conductivity of PANI (~0.1 W/mK[18]). Since the final equilibrium temperature depends on the total amount of heat generated and the heat transfer efficiency to external surface, it is not surprising to observe the relatively lower equilibrium temperature but higher reaction efficiency of CP30 than that of CNTs.

The ratio of CNTs and PANI in the composites affects both shell morphology and thickness. As discussed above, rough surface structure would reduce electromagnetic wave reflection and facilitate the translation of microwave energy to heat. Considering electrically conductive

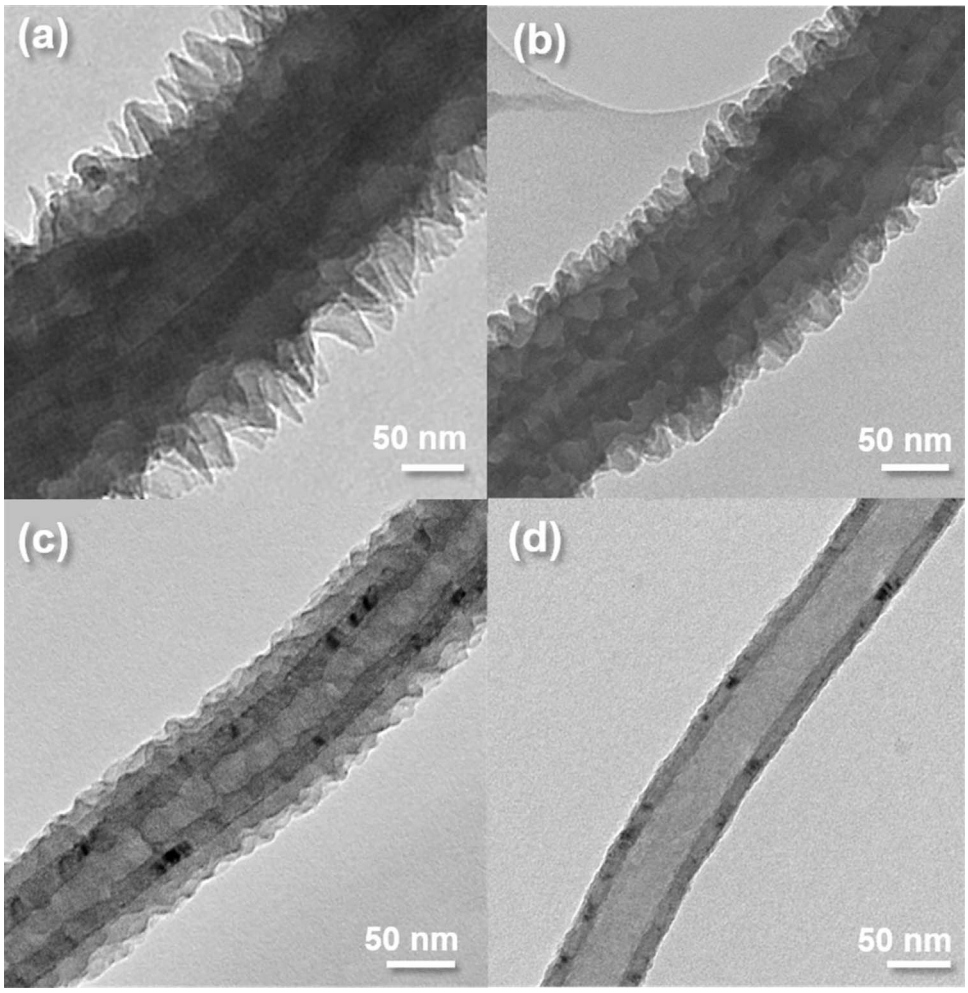

Fig. 2. TEM image of (a) CP10, (b) CP20, (c) CP30 and (d) CP40.

Table 1
Summary of structure information and elemental composition.

	SA ($m^2 g^{-1}$)	D_{pore} (nm)	V_{pore} ($cm^3 g^{-1}$)	PANI Thickness (nm)	Chemical composition (wt%)		
					C	N	S
Polyaniline	22.1	5.6	0.04	–	53.7	10.5	5.4
CP10	23.5	5.3	0.04	122	78.1	4.3	3.3
CP20	26.8	5.4	0.05	74	81.8	3.2	3.1
CP30	29.0	5.3	0.05	34	83.6	2.4	3.8
CP40	28.8	5.3	0.04	< 5	90	1.8	1.7
CNTs	33.7	5.1	0.06	–	97.9	–	1.0

SA: surface area; D_{pore}: pore diameter; V_{pore}: pore volume.

nature of PANI, the shell thickness will definitely affect the overall microwave absorption of the composite catalyst. Thicker shell absorbs more microwave energy that partially blocks microwave translation to CNTs core. Moreover, thicker shell is certainly not favored in term of heat conduction from the inner core to the outer shell due to the low thermal conductivity of PANI. The continuous increase of the equilibrium temperature from CP10 to CP30 in Fig. 4(a) is mainly due to the increasing fraction of CNTs and thinner PANI shell. The temperature drop of CP40 is mainly attributed to its smooth shell structure that reflects the electromagnetic wave. The effect of surface structure on the microwave transmission/reflection is schematically presented in Fig. 5, where most of the electromagnetic wave can be translated into the material on a rough surface while reflected on a smooth surface. R. Che et al. also found that a TiO_2 shell with nanosheet structure could increase absorption/scattering during microwave propagating, which helps to enhance the microwave absorption capability [39]. Among all the core/shell catalysts, CP30 acquires the highest reactivity as evidenced by the 81 mol% fructose conversion (Fig. S5) and ~60 mol% HMF yield in 30 min.

Besides the ratio of reactants, PANI shell thickness and morphology can be tuned by polymerization reaction as well through adjusting the concentration of oxidant APS. Fig. 6(a–d) shows the TEM images of core-shell structured catalysts with continuously increased PANI shell thickness and surface roughness. By using a small amount of APS (0.4 mmol), a thin PANI shell layer of less than 5 nm is formed on the CNT surface, Fig. 6(a). Such thin layer of PANI formation could be ascribed to the incomplete polymerization since low APS concentration will form low molecular weight oligomers [44]. These oligomers typically show poor electrical conductivity and thus poor permittivity [45] that impedes the microwave absorption of inner CNT. As a result, the CP30-0 gives the lowest system equilibrium temperature, Fig. 6(e). With increasing APS concentration to 1.3, 2.2 and 3.1 mmol, the PANI shell thickness continuously increases to 32, 51 and 56 nm, Fig. 6(b–d). Together with this process, the weight percentage of N element goes up from 2.4 (CP30-1) to 4.4% (CP30-2) and then drops down to 3.4% (CP30-3), Table 2.

The larger N percentage in CP30-2 well corresponds to its thicker PANI layer on CNT surface. Compared to the CP30-3 with similar thickness but loose shell structure, it is not surprising to observe the relatively higher N content in CP30-2. While synthesizing CP30-3, unattached PANI nanofibers were observed in the aqueous phase rather than growing on the CNTs. Therefore, the actual PANI percentage in the

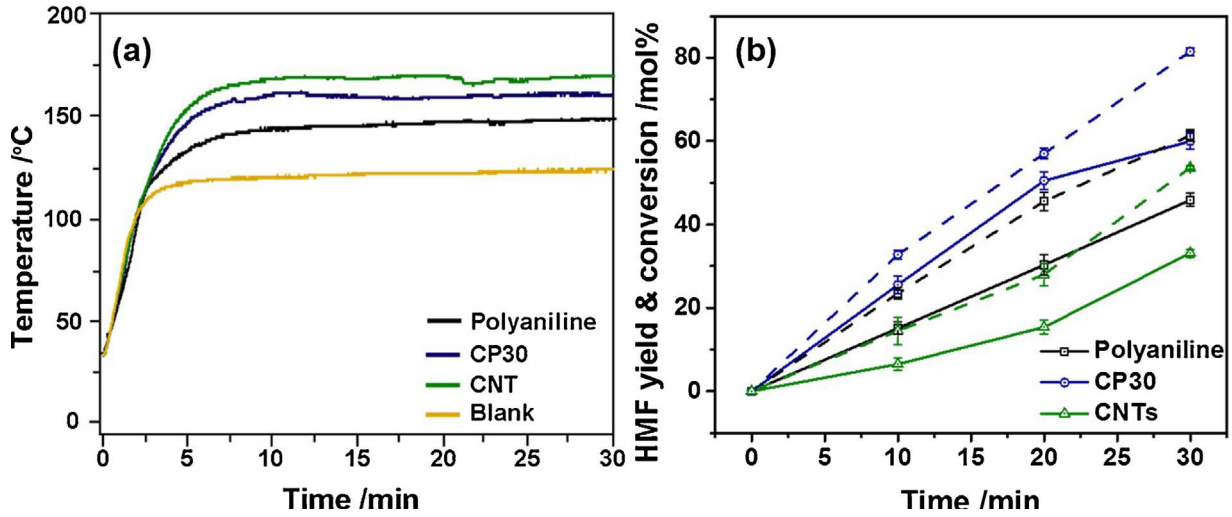

Fig. 3. (a) System temperature profile and (b) HMF yield (solid line) and fructose conversion (dash line) as a function of reaction time by using polyaniline, CNT/PANI (CP30) and CNTs catalysts. Reaction condition: [fructose] = 0.55 mmol, [catalysts] = 12.5 mg/mL, input power = 15 W.

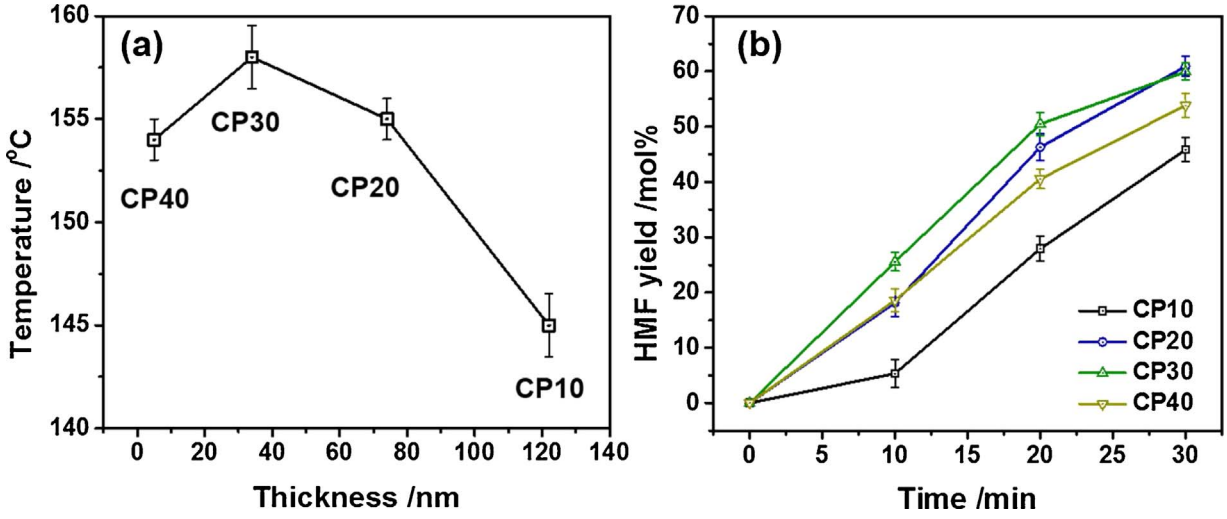

Fig. 4. (a) System equilibrium temperature and (b) HMF yield as a function of time at different CNT/PANI ratios. Reaction condition: [fructose] = 0.55 mmol, [catalysts] = 12.5 mg/mL, input power = 15 W.

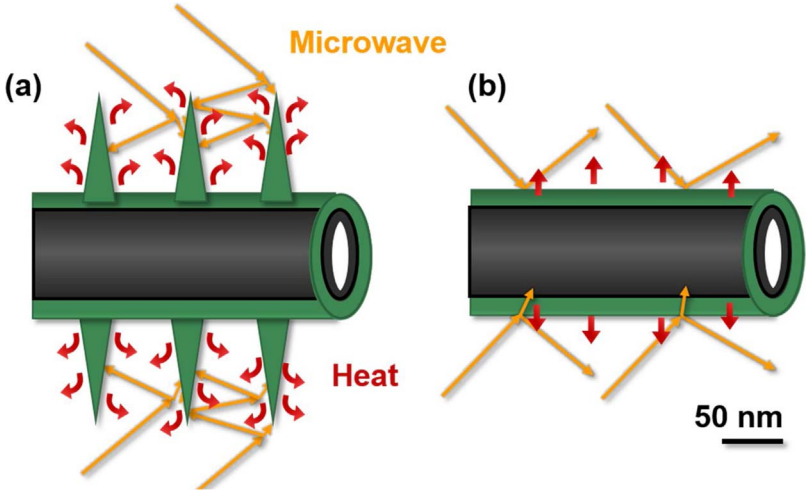

Fig. 5. Scheme of microwave transmission and reflection on (a) nanoflake surface and (b) flat surface.

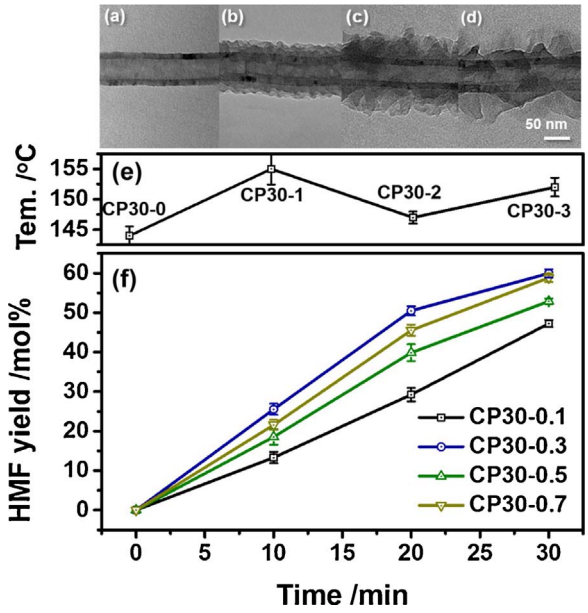

Fig. 6. TEM image of (a) CP30-0, (b) CP30-1, (c) CP30-2 and (d) CP30-3, (e) system temperature and (f) HMF yield. Reaction condition: [fructose] = 0.55 mmol, [catalyst] = 12.5 mg/mL, input power = 15 W. (a–d uses 0.4, 1.3, 2.2 and 3.1 mmol APS).

Table 2
Structure information and elemental composition of CP30-X catalyst.

	SA ($m^2\ g^{-1}$)	D_{pore} (nm)	V_{pore} ($cm^3\ g^{-1}$)	PANI thickness (nm)	Chemical composition (wt%)		
					N	C	S
CP30-0	33.1	5.3	0.05	< 6	1.9	88.5	3.3
CP30-1	29.0	5.3	0.05	34	2.4	83.6	3.8
CP30-2	24.6	5.4	0.04	53	4.4	75.7	3.8
CP30-3	26.1	5.4	0.04	56	3.4	80.6	3.3

SA: surface area; D_{pore}: pore diameter; V_{pore}: pore volume.

composites is less than expected. Comparing the surface structure of CP30-2 and CP30-3, CP30-3 acquires larger PANI flakes those are sparsely distributed on the CNT surface. Such structure is beneficial to transmit microwave and favors microwave reflection within the surface structure to improve the overall translation of microwave to heat. With

Table 3
Energy efficiency of HMF production at different power input conditions.

Catalyst	Time (min)	Energy efficiency (mmol $kJ^{-1}\ L^{-1}$)				
		11 W	13 W	15 W	17 W	19 W
CP30	10	0.8	2.2	3.9	6.3	7.6
CP30	20	1.1	2.0	3.9	4.8	4.4
CP30	30	1.2	2.0	3.1	3.0	2.6
PANI	30	0.8	1.4	2.6	2.7	2.5
CNTs	30	0.1	0.2	0.8	1.0	1.8

that, these catalysts show different equilibrium temperatures with CP30-1 the highest and follow by CP30-3, CP30-2 and CP30-0, Fig. 6(e). The HMF yield is highly consistent with the equilibrium temperature, where higher temperature leads to larger HMF yield, Fig. 6(f).

In terms of energy efficiency, input power needs to be optimized to maximize HMF yield and also minimize side reactions. In this work, microwave power output is adjusted from 11 to 19 W. Apparently, larger power input leads to a higher temperature ramping rate and system equilibrium temperature, Fig. 7(a). The input power greatly affects the HMF yield. For example, in the first 10 min of reaction, the HMF yield is only 4 mol% with 11 W input power, while it sharply increases to 63 mol% by increasing input power to 19 W. To compare the energy efficiency of the reaction, η is defined in Eq. (3) that describes the amount of HMF produced by consuming per unit of work.

$$\text{Energy efficiency } \eta = \frac{[HMF]}{P \cdot t \cdot V} \tag{3}$$

where P is input power of microwave, t is elapsed time and V is volume of reaction solution. The η values calculated at different power levels with different reaction times were summarized in Table 3. The highest energy efficiency of 7.6 mmol $kJ^{-1}\ L^{-1}$ was achieved by using CP30 catalyst with power level of 19 W and reaction time of 10 min. It is worth mentioning that η decreases with longer reaction time since larger input power accelerates the rehydration reaction of HMF to levulinic acid. The maximum η values for PANI and CNTs are 2.7 and 1.8 mmol $kJ^{-1}\ L^{-1}$, respectively. These results demonstrate the synergistic effect of PANI and CNTs in serving as microwave responsive catalyst.

Even though heterogeneous catalysis has the advantage of catalyst separation, it still remains a great challenge when catalysts are in nanometer size. In this work, the separation of pure PANI catalyst and CNT/PANI composites from reaction media was comparatively

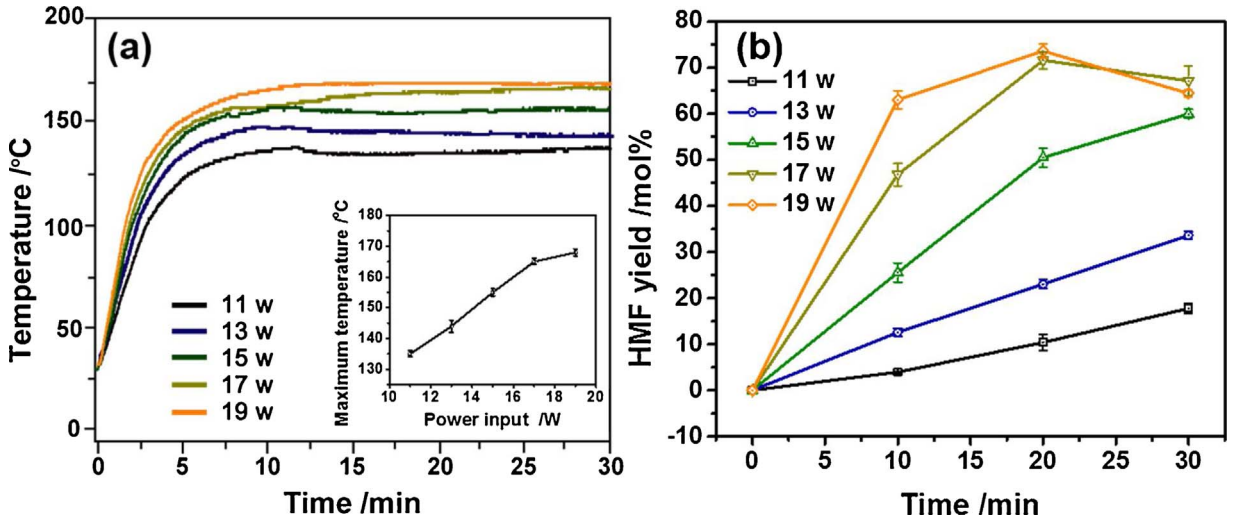

Fig. 7. Effect of input power on (a) system temperature and (b) HMF yield. Reaction condition: [fructose] = 0.55 mmol, [CP30] = 12.5 mg/mL. The inset of (a) is a plot of the maximum system temperature *vs.* input power.

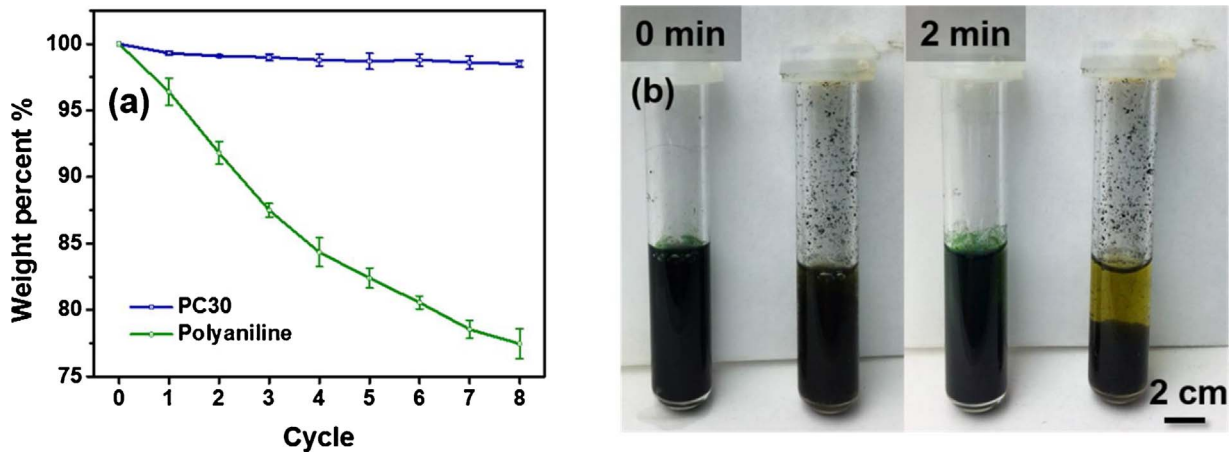

Fig. 8. (a) Sedimentation for 2 min in product suspensions and (b) catalysts retain amount of CP30 and polyaniline. Reaction conditions: [fructose] = 55 mmol, [catalyst] = 12.5 mg/mL, power: 15 W, reaction time:30 min.

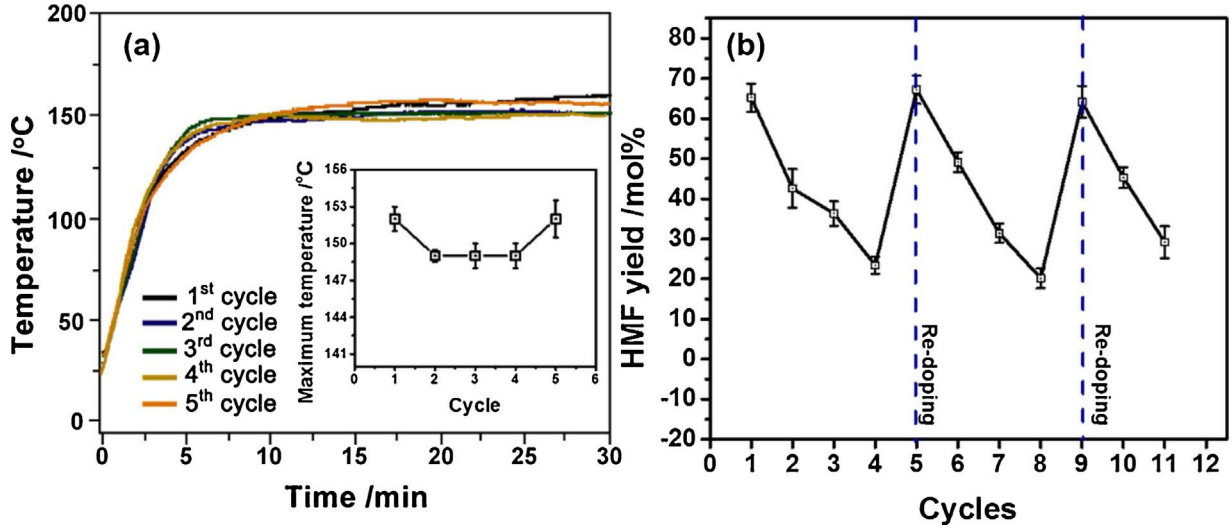

Fig. 9. Recycling of CP30 catalystfor the catalyticdehydration of fructose to HMF. Reaction conditions: [fructose] = 55 mmol, [catalyst] = 12.0 mg/mL, power: 15 W and reaction time:30 min.

investigated. Specifically, the catalysts were separated by centrifugal method after each reaction cycle and the mass of catalyst after each separation process was continuously monitored. As showed in Fig. 8(a), more than 97% of CP30 was retained after 8 cycles of reaction, while only 77% of PANI can be recycled. Fig. 8(b) shows the reaction mixture immediately after reaction and after 2 min sedimentation. Apparently, CP30 can be easily separated from the reaction mixture while pure PANI remains a uniform suspension. Therefore, such integration of functional PANI onto CNT core facilitates its separation from the reaction mixture and reduces catalyst loss during catalyst separation and recycling, Fig. 8(b)

Doping acid on PANI backbone is the major active site for the fructose conversion reaction. During reaction, these acidic sites will be gradually consumed and lead to reduced catalyst activity. Meanwhile, the de-doped PANI would lose its electrical conductivity and affect its microwave absorption capacity. Fig. 9(a) shows the temperature profiles of the reactions with the same catalyst of CP30. The solution equilibrium temperature drops from 153 to 149 °C in the 2nd cycle and stabilized in the 3rd and 4th cycles. Even though cycles 2–4 show similar equilibrium temperature, the HMF yield continuously drops from 65 (1st cycle) to 25 mol% (4th cycle), Fig. 9(b). These results further reveal that reaction temperature is not the only factor that determines HMF yield, the amount of doping acid on PANI backbone could be even more important in this reaction. After the 4th cycle of reaction, the catalyst was separated and re-doped by soaking in 1.0 M sulfuric acid. After rinsing off surface residues, the re-doped CP30 shows a similar acidity as fresh catalyst. The equilibrium temperature goes back to 153 °C (inset of Fig. 9a) and HMF yield increase to 66 mol% (Fig. 9b). The catalyst was continuously tested with additional cycles and similar performance is remained ever being activated again in the 9th cycle.

Additionally, CP30 was tested for the dehydration reaction with glucose and sucrose reactants, Fig. S6. The lower conversion percentage and HMF yield from glucose than that from fructose can be attributed to the mutarotation and isomerization of glucose before dehydration reaction occurs [46,47]. The higher HMF yield with sucrose is due to the further hydrolysis of fructose and glucose units, which are concurrently dehydrated to HMF [48].

4. Conclusions

To sum up, core/shell structured CNT/PANI catalysts were successfully synthesized of different PANI shell thickness and surface morphology. These materials show synergistically enhanced microwave adsorption property and demonstrate highly energy-efficient conversion of saccharide to HMF. Catalysts with a thinner shell and rough surface texture are favorable to reach high reaction temperature, reactant conversion and product yield. The highest energy efficiency of 7.6 mmol kJ^{-1} L^{-1} is reached in 10 min with CP30 catalyst and 19 W

input power. Increasing reaction time leads to the formation of side products and negatively affects the HMF yield. The packing of PANI shell on CNT core facilitates its separation from reaction mixture with less catalyst loss. Besides, these catalysts can be easily reactivated by a simple re-doping process. This study opens up a new opportunity to enhance energy efficiency in saccharide-HMF conversion reactions and promotes the economic feasibility of such reactions in practice.

Acknowledgements

Acknowledgement is made to the Donors of the American Chemical Society Petroleum Research Fund (#55570-DNI10) and NSF (CBET-1603264). The authors appreciate the instrument support and postdoc assistance Nicholas Callow from Prof. Lukwang Ju's group. HRTEM was performed at the Liquid Crystal Institute, Kent State University supported by the Ohio Research Scholars Program Research Cluster on Surfaces in Advanced Materials. The authors appreciate the technical support from Dr. Min Gao with HRTEM.

Appendix A. Supplementary data

Supplementary data associated with this article can be found, in the online version, at http://dx.doi.org/10.1016/j.apcatb.2017.08.066.

References

[1] I. Jiménez-Morales, A. Teckchandani-Ortiz, J. Santamaría-González, P. Maireles-Torres, A. Jiménez-López, Selective dehydration of glucose to 5-hydroxymethylfurfural on acidic mesoporous tantalum phosphate, Appl. Catal. B 144 (2014) 22–28.
[2] X. Zhang, D. Zhang, Z. Sun, L. Xue, X. Wang, Z. Jiang, Highly efficient preparation of HMF from cellulose using temperature-responsive heteropolyacid catalysts in cascade reaction, Appl. Catal. B 196 (2016) 50–56.
[3] J. Luo, J.D. Lee, H. Yun, C. Wang, M. Monai, C.B. Murray, P. Fornasiero, R.J. Gorte, Base metal-Pt alloys: a general route to high selectivity and stability in the production of biofuels from HMF, Appl. Catal. B 199 (2016) 439–446.
[4] T. Ji, L. Chen, L. Mu, R. Yuan, M. Knoblauch, F.S. Bao, Y. Shi, H. Wang, J. Zhu, Green processing of plant biomass into mesoporous carbon as catalyst support, Chem. Eng. J. 295 (2016) 301–308.
[5] L. Chen, T. Ji, L. Brisbin, J. Zhu, Hierarchical porous and high surface area tubular carbon as dye adsorbent and capacitor electrode, ACS Appl. Mater. Interfaces 7 (2015) 12230–12237.
[6] L. Chen, T. Ji, R. Yuan, L. Mu, L. Brisbin, J. Zhu, Unveiling mesopore evolution in carbonized wood: interfacial separation, migration, and degradation of lignin phase, ACS Sustain. Chem. Eng. 3 (2015) 2489–2495.
[7] J. Zhu, M. Chen, H. Qu, Z. Luo, S. Wu, H.A. Colorado, S. Wei, Z. Guo, Magnetic field induced capacitance enhancement in graphene and magnetic graphene nanocomposites, Energy Environ. Sci. 6 (2013) 194–204.
[8] G. Li, Z. Sun, Y. Yan, Y. Zhang, Y. Tang, Direct transformation of HMF into 2, 5-diformylfuran and 2, 5-dihydroxymethylfuran without an external oxidant or reductant, ChemSusChem (2016) 494–498.
[9] A. Dibenedetto, M. Aresta, L. di Bitonto, C. Pastore, Organic carbonates efficient extraction solvents for the synthesis of HMF in aqueous media with cerium phosphates as catalysts, ChemSusChem 9 (2016) 118–125.
[10] F.D. Pileidis, M.M. Titirici, Levulinic acid biorefineries: new challenges for efficient utilization of biomass, ChemSusChem 9 (2016) 562–582.
[11] G. Yi, S.P. Teong, Y. Zhang, Base-free conversion of 5-hydroxymethylfurfural to 2, 5-furandicarboxylic acid over a Ru/C catalyst, Green Chem. 18 (2016) 979–983.
[12] F. Wang, H.-Z. Wu, C.-L. Liu, R.-Z. Yang, W.-S. Dong, Catalytic dehydration of fructose to 5-hydroxymethylfurfural over Nb_2O_5 catalyst in organic solvent, Carbohydr. Res. 368 (2013) 78–83.
[13] A. Osatiashtiani, A.F. Lee, D.R. Brown, J.A. Melero, G. Morales, K. Wilson, Bifunctional SO_4/ZrO_2 catalysts for 5-hydroxymethylfufural (5-HMF) production from glucose, Catal. Sci. Technol. 4 (2014) 333–342.
[14] C. Tian, X. Zhu, S.-H. Chai, Z. Wu, A. Binder, S. Brown, L. Li, H. Luo, Y. Guo, S. Dai, Three-phase catalytic system of H_2O, ionic liquid, and $VOPO_4$-SiO_2 solid acid for conversion of fructose to 5-hydroxymethylfurfural, ChemSusChem 7 (2014) 1703–1709.
[15] R.J. van Putten, J.C. van der Waal, M. Harmse, H.H. van de Bovenkamp, E. de Jong, H.J. Heeres, A comparative study on the reactivity of various ketohexoses to furanics in methanol, ChemSusChem 9 (2016) 1827–1834.
[16] T. Okuhara, Water-tolerant solid acid catalysts, Chem. Rev. 102 (2002) 3641–3666.
[17] X. Zhang, D.O. Hayward, C. Lee, D.M.P. Mingos, Microwave assisted catalytic reduction of sulfur dioxide with methane over MoS_2 catalysts, Appl. Catal. B 33 (2001) 137–148.
[18] A.A. Rosatella, S.P. Simeonov, R.F. Frade, C.A. Afonso, 5-Hydroxymethylfurfural (HMF) as a building block platform: biological properties, synthesis and synthetic applications, Green Chem. 13 (2011) 754–793.
[19] A.M. Rodriguez, P. Prieto, A. de la Hoz, A. Diaz-Ortiz, D.R. Martin, J.I. Garcia, Influence of polarity and activation energy in microwave-assisted organic synthesis (MAOS), Chemistryopen 4 (2015) 308–317.
[20] A.M. Schwenke, S. Hoeppener, U.S. Schubert, Synthesis and modification of carbon nanomaterials utilizing microwave heating, Adv. Mater. 27 (2015) 4113–4141.
[21] R. Carrasquillo-Flores, M. Käldström, F. Schüth, J.A. Dumesic, R. Rinaldi, Mechanocatalytic depolymerization of dry (ligno) cellulose as an entry process for high-yield production of furfurals, ACS Catal. 3 (2013) 993–997.
[22] X. Qi, M. Watanabe, T.M. Aida, R.L. Smith Jr., Catalytic dehydration of fructose into 5-hydroxymethylfurfural by ion-exchange resin in mixed-aqueous system by microwave heating, Green Chem. 10 (2008) 799–805.
[23] M. Omri, G. Pourceau, M. Becuwe, A. Wadouachi, Improvement of gold-catalyzed oxidation of free carbohydrates to corresponding aldonates using microwaves, ACS Sustain. Chem. Eng. 4 (2016) 2432–2438.
[24] C.O. Kappe, Controlled microwave heating in modern organic synthesis, Angew. Chem. Int. Ed. 43 (2004) 6250–6284.
[25] R. Vadivambal, D. Jayas, Non-uniform temperature distribution during microwave heating of food materials-a review, Food Bioprocess Technol. 3 (2010) 161–171.
[26] R. Che, L.M. Peng, X.F. Duan, Q. Chen, X. Liang, Microwave absorption enhancement and complex permittivity and permeability of Fe encapsulated within carbon nanotubes, Adv. Mater. 16 (2004) 401–405.
[27] F. Wen, F. Zhang, Z. Liu, Investigation on microwave absorption properties for multiwalled carbon nanotubes/Fe/Co/Ni nanopowders as lightweight absorbers, J. Phys. Chem. C 115 (2011) 14025–14030.
[28] X. Liu, Z. Zhang, Y. Wu, Absorption properties of carbon black/silicon carbide microwave absorbers, Compos. Part B 42 (2011) 326–329.
[29] C. Wang, X. Han, P. Xu, X. Zhang, Y. Du, S. Hu, J. Wang, X. Wang, The electromagnetic property of chemically reduced graphene oxide and its application as microwave absorbing material, Appl. Phys. Lett. 98 (2011) 072906.
[30] M.-S. Cao, W.-L. Song, Z.-L. Hou, B. Wen, J. Yuan, The effects of temperature and frequency on the dielectric properties, electromagnetic interference shielding and microwave-absorption of short carbon fiber/silica composites, Carbon 48 (2010) 788–796.
[31] C. Blawert, H. Kalvelage, B. Mordike, G. Collins, K. Short, Y. Jirásková, O. Schneeweiss, Nitrogen and carbon expanded austenite produced by PI^3, Surf. Coat. Technol. 136 (2001) 181–187.
[32] J.S. Church, N.W. Cant, D.L. Trimm, Stabilisation of aluminas by rare earth and alkaline earth ions, Appl. Catal. A 101 (1993) 105–116.
[33] P. Saini, V. Choudhary, B. Singh, R. Mathur, S. Dhawan, Polyaniline–MWCNT nanocomposites for microwave absorption and EMI shielding, Mater. Chem. Phys. 113 (2009) 919–926.
[34] R. Yuan, H. Wang, T. Ji, L. Mu, L. Chen, Y. Zhu, J. Zhu, Superhydrophobic polyaniline hollow spheres with mesoporous brain-like convex-fold shell textures, J. Mater. Chem. A 3 (2015) 19299–19303.
[35] L. Mu, Y. Shi, T. Ji, L. Chen, R. Yuan, H. Wang, J. Zhu, Ionic grease lubricants: protic [triethanolamine][oleic acid] and aprotic [choline][oleic acid], ACS Appl. Mater. Interfaces 8 (2016) 4977–4984.
[36] J. Zhu, S. Wei, L. Zhang, Y. Mao, J. Ryu, A.B. Karki, D.P. Young, Z. Guo, Polyaniline-tungsten oxide metacomposites with tunable electronic properties, J. Mater. Chem. 21 (2011) 342–348.
[37] T. Ji, L. Chen, M. Schmitz, F.S. Bao, J. Zhu, Hierarchical macrotube/mesopore carbon decorated with mono-dispersed Ag nanoparticles as a highly active catalyst, Green Chem. 17 (2015) 2515–2523.
[38] X. Zheng, L. Wang, R. Wang, T. Ge, T. Ishugah, Thermal conductivity, pore structure and adsorption performance of compact composite silica gel, Int. J. Heat Mass Transf. 68 (2014) 435–443.
[39] S.H. Bhavnani, A.E. Bergles, Effect of surface geometry and orientation on laminar natural convection heat transfer from a vertical flat plate with transverse roughness elements, Int. J. Heat Mass Transf. 33 (1990) 965–981.
[40] G. Li, T. Xie, S. Yang, J. Jin, J. Jiang, Microwave absorption enhancement of porous carbon fibers compared with carbon nanofibers, J. Phys. Chem. C 116 (2012) 9196–9201.
[41] T. Ji, R. Tu, L. Mu, X. Lu, J. Zhu, Enhancing energy efficiency in saccharide-HMF conversion with core/shell structured microwave responsive catalysts, ACS Sustain. Chem. Eng. 5 (2017) 4352–4358.
[42] M.-S. Cao, J. Yang, W.-L. Song, D.-Q. Zhang, B. Wen, H.-B. Jin, Z.-L. Hou, J. Yuan, Ferroferric oxide/multiwalled carbon nanotube vs polyaniline/ferroferric oxide/multiwalled carbon nanotube multiheterostructures for highly effective microwave absorption, ACS Appl. Mater. Interfaces 4 (2012) 6949–6956.
[43] D.A. Makeiff, T. Huber, Microwave absorption by polyaniline–carbon nanotube composites, Synth. Met. 156 (2006) 497–505.
[44] T. Ji, W. Cao, L. Chen, L. Mu, H. Wang, X. Gong, X. Lu, J. Zhu, Confined molecular motion across liquid/liquid interfaces in a triphasic reaction towards free-standing conductive polymer tube arrays, J. Mater. Chem. A 4 (2016) 6290–6294.
[45] R.B. Yang, P.M. Reddy, C.J. Chang, P.A. Chen, J.K. Chen, C.C. Chang, Synthesis and characterization of Fe_3O_4/polypyrrole/carbon nanotube composites with tunable microwave absorption properties: role of carbon nanotube and polypyrrole content, Chem. Eng. J. 285 (2016) 497–507.
[46] S. De, S. Dutta, B. Saha, Microwave assisted conversion of carbohydrates and biopolymers to 5-hydroxymethylfurfural with aluminium chloride catalyst in water, Green Chem. 13 (2011) 2859–2868.
[47] S. Despax, B. Estrine, N. Hoffmann, J. Le Bras, S. Marinkovic, J. Muzart, Isomerization of d-glucose into d-fructose with a heterogeneous catalyst in organic solvents, Catal. Commun. 39 (2013) 35–38.
[48] Q. Wu, Y. Yan, Q. Zhang, J. Lu, Z. Yang, Y. Zhang, Y. Tang, Catalytic dehydration of carbohydrates on in situ exfoliatable layered niobic acid in an aqueous system under microwave irradiation, ChemSusChem 6 (2013) 820–825.